Optical properties of stretched polymer dispersed liquid crystal films: Angle-dependent polarized light scattering

Oleg A. Aphonin[a]

[a] Department of Physics, University of Saratov, Saratov, Russia

PLEASE SCROLL DOWN FOR ARTICLE

Optical properties of stretched polymer dispersed liquid crystal films: angle-dependent polarized light scattering

by OLEG A. APHONIN

Department of Physics, University of Saratov, Astrakhanskaya 83,
410071 Saratov, Russia

A systematic experimental study of the polarization-dependent light scattering properties of uniaxially stretched polymer dispersed liquid crystal (PDLC) films with the bipolar director field structure in the micron-sized nematic droplets is presented. The space distribution of the scattered intensity as a function of the incident and scattered optical polarization, as well as the degree and azimuth of polarization of the scattered light have been measured, and the results are discussed in terms of physical parameters related to the sample structure, such as molecular alignment, droplet size, shape, orientation, etc. The main factors determining the light polarizing ability of an ordered PDLC film are discussed. On the basis of the results obtained, some potential display applications of a stretched PDLC film are proposed. In particular, the reasons are given for using such a film as a polarizing diffuser for backlit twisted nematic LCDs.

1. Introduction

Currently there is considerable interest in the study of the optical properties of polymer dispersed liquid crystals (PDLCs), induced by a wide range of potential optoelectronic applications of this new class of composite materials [1]. An interesting branch is the family of uniaxially ordered PDLC systems of various morphologies, including the LC-droplet type, polymer network type, and gel type morphologies, which are highly anisotropic and exhibit a strong polarization effect in light scattering [2–9]. Thin films of these materials are promising for effective non-absorptive polarizers, polarization-sensitive light shutters, variable diffusers, etc.

Optimizing the performance of a PDLC polarizer for a specific application requires an in-depth knowledge of the optical properties of ordered PDLC systems. In our previous publication on this topic [7], we have studied, both theoretically and experimentally, the basic mechanisms determining the creation of optical anisotropy in a uniaxially stretched PDLC film having the droplet-type morphology with the bipolar director field configuration in the micron-sized nematic droplets. Most attention, however, has been concentrated on examination of the anistropic transmittance of the film, while the investigation of the large angle-scattering was not included. In this contribution we present a more detailed experimental study to establish the principal polarization-dependent light scattering properties of a stretched PDLC film for an arbitrary direction of the scattered light.

2. Experimental

2.1. Sample preparation

The PDLC films were prepared by the polymer encapsulation method [10, 11]. 1 g of biphenyl nematic mixture SZK-1 (similar to BDH E7 LC mixture; available from Niopik, Moscow) was emulsified with a laboratory stirrer in 33 g of a 10 per cent aqueous solution of a polyvinyl alcohol (PVA)/glycerol mixture, with a glycerol content of 10 per cent with reference to pure PVA weight. Glycerol was used as a plasticizer to increase the elasticity of the polymer matrix. The droplet size distribution in the emulsion, measured by optical microscopy, covered the droplet diameter range from approximately 1 to 8 μm, with a mean diameter of about 3 μm. The emulsion was then coated onto a clear glass substrate by drawing a knife edge with adjustable gap over the substrate surface; the upper surface of the film was left free and the solvent (water) was evaporated in a clean environment. The volume fraction of droplets in dried films was approximately 0·3, the film thickness being about 40 μm. (Note that the above-listed parameters are related to the unstretched PDLC films. The morphological changes in stretched samples will be discussed in § 4.1.) The index match resulting from the materials used was quite good: for the wavelength 633 nm, which was utilized in all our light scattering experiments, the principal refractive indices of the liquid crystal were $n_o = 1·52$, $n_e = 1·73$, whereas the refractive index of the unstretched polymer matrix was $n_m \approx 1·51$ (all values are for 20°C).

For light scattering measurements, rectangular specimens 30 × 20 mm² were cut from sheets of the PDLC film separated from the substrate, and these were placed in a special mechanical unit providing controllable unidirectional stretching of the film in the range from 0 to 300 per cent with reference to the initial film length. It was found necessary to sandwich the elongated samples between microscope cover glasses, using glycerol as an immersion fluid, to prevent scattering by surface defects from making an undue contribution [7].

2.2. Scattering geometry and measured parameters

The scattering geometry is shown schematically in figure 1. Quite sufficient information on the scattering by the film is contained in four principal scattered intensities, $I_{\|\|}$, $I_{\perp\|}$, $I_{\perp\perp}$ and $I_{\|\perp}$, where the pair of indices $\|$ and $\perp$ denote the polarizer–analyser combinations, with respect to the reference planes, from which the corresponding intensities can be measured (see [12–14] for a more detailed treatment). These intensities can be regarded as scattering cross-sections for a system of nematic droplets. Additional characteristics to be discussed are the depolarization coefficients for $\|$- and $\perp$-polarized components of the incident beam, defined as

$$\Delta_\| = I_{\perp\|}/I_{\|\|}, \quad \Delta_\perp = I_{\|\perp}/I_{\perp\perp}. \qquad (1)$$

The next necessary parameter is the degree of linear polarization of the scattered beam for unpolarized incident light, which can be treated as a measure of the light polarizing ability of a stretched PDLC film and is given by

$$P = \frac{I_{\|u} - I_{\perp u}}{I_{\|u} + I_{\perp u}}, \qquad (2)$$

where $I_{\|u} = (I_{\|\|} + I_{\|\perp})/2$ and $I_{\perp u} = (I_{\perp\perp} + I_{\perp\|})/2$ and are the principal scattered intensities for the unpolarized incident light. Finally, one should determine the azimuth
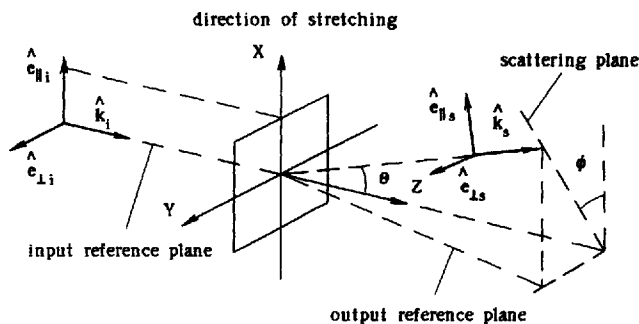
of polarization of the scattered beam with respect to the output reference plane.

2.3. Apparatus and measurement procedures

The angular dependencies of the scattered light intensity were measured with the experimental set-up shown schematically in figure 2. Linear polarized monochromatic light from a stabilized 20 mW helium–neon laser ($\lambda = 632\cdot8$ nm) provided the incident light beam that passed through a chopper, beam expanding spatial filter, collimating lens, 5 mm diameter iris diaphragm and neutral density light filter and was directed onto a polarizing filter consisting of a quarter-wave plate and linear prism polarizer. The latter combination provided the ability to control the azimuth of the polarization vector of the incident light without loss of intensity by rotating the polarizer about its normal. The laser beam was incident normally on the PDLC sample which was placed in a rotary sample holder mounted just above the axis of a precise goniometer.

Scattered light passed through a linear analyser and was collected with a 100 mm focal-length lens on to a low noise Si-photodiode detector. A 1·7 mm diameter aperture in the focal plane of the collecting lens ensured that only light scattered within a cone of 0·5° half-angle about the optical axis of the detection system would reach the detector. The entire detection system (analyser, lens, focal-plane aperture and detector) was placed on the rotating arm of the goniometer so that the scattered light intensity could be measured as a function of the scattering angle, θ, over the range $0° \leq |\theta| \leq 170°$ (the range $170° < |\theta| \leq 180°$ was inaccessible in our experiments). The photodector output voltage was measured using a lock-in amplifier tuned to the 1 kHz chopping frequency. The use of calibrated neutral density filters in the incident beam permitted the detector response to be linear over the entire range of scattered light levels attained in our experiments. The power received by the detector at each scattering angle was normalized to the incident laser intensity taken at $\theta = 0°$ when no sample was present.

direction of stretching

Figure 1. Coordinate system used for describing the scattering of normally incident light by a stretched PDLC film. $\hat{e}_{\|i}$, $\hat{e}_{\perp i}$ and $\hat{e}_{\|s}$, $\hat{e}_{\perp s}$ are unit vectors representing the components of incident and scattered beams, respectively, polarized parallel ($\|$) and perpendicular ($\perp$) to the corresponding reference planes.
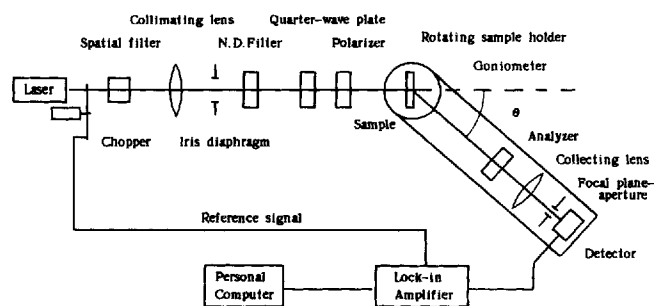

Figure 2. Schematic diagram of experimental setup for angle-dependent light scattering measurements.

To represent the spatial distribution of principal scattered intensities, $I_{\|\|}$, $I_{\perp\|}$, $I_{\perp\perp}$ and $I_{\|\perp}$, the corresponding scattering diagrams, both for the forward ($0° \leqslant |\theta| \leqslant 90°$) and backward ($90° \leqslant |\theta| \leqslant 180°$) hemispheres were measured. These diagrams are the families of curves of constant intensity in polar coordinates (so called isophotes), obtained by successively varying the azimuthal angle ϕ every $1°$, rotating the sample holder, and simultaneously measuring the angle θ, providing the condition of constant signal from the detector. As the azimuth of the scattering plane was changed by rotating the sample holder, the polarizer and analyser were readjusted to have fixed orientation with respect to the reference planes. The conventional angular spectra for principal scattered intensities were measured by varying the angle θ from $0°$ to $170°$ every $1°$ below $\theta = 30°$ and every $2°$ above, the azimuthal angle, ϕ, being fixed every $5°$. The latter procedure was also used in measuring the angular distribution of the degree of polarization, P, given by equation (2). The unpolarized light was modelled by the circularly polarized incident wave obtained by removing the input linear polarizer from the optical scheme. Because the first two Stokes parameters for a circularly polarized wave are the same as for unpolarized light [12], the corresponding principal scattered intensities were indistinguishable experimentally. The azimuth of polarization was determined simultaneously with P by rotating the analyser to minimize the intensity received by the detector. The collection of data was completely automated through the use of a personal computer.

3. Results

Our major findings are shown in figures 4–9, 11 and 12. Figures 3 and 10 are auxiliary and illustrate the morphological modifications in a PDLC film upon stretching (see below). The light scattering diagrams for the principal intensities scattered by the stretched PDLC film into the forward and backward hemispheres are presented in figures 4 and 5, respectively. Only one quadrant $0° \leqslant |\phi| \leqslant 90°$ is shown, since the scattering patterns for the others are symmetric about the two principal scattering planes: the meridional XZ plane ($\phi = 0°$) (see figure 1) and the equatorial YZ plane ($\phi = 90°$). The angular scattering spectra and depolarization coefficients for these planes are shown in figure 6. The results for the unstretched PDLC film are also presented for comparison. Figure 7 represents the angular spectra on an expanded scale for scattering angles below $10°$, and figure 8 shows the dependencies of the principal film transmittances on relative film elongation. Figure 9 illustrates the energy redistribution between the principal scattered intensities on stretching, and the data giving information about the angular distribution of the degree of polarization of the scattered light are displayed in figures 11 and 12. Since potential applications

of stretched PDLC films are expected to utilize planar or nearly planar samples in air, we have not made any boundary corrections associated with the refraction and reflection of polarized scattered light at the sample–air interfaces [15, 16].

4. Discussion

4.1. Changes in the morphology of a PDLC film upon stretching

To be able to interpret the light scattering behaviour of a stretched PDLC film in terms of physical parameters related to the sample structure, it is necessary to cover first the changes in the film morphology. Studies of the microstructure of our PVA based PDLC samples by polarizing optical microscopy [7, 17] have testified that the nematic material in the droplets adopted the bipolar director field configuration with two surface point defects classified as boojums on opposite sides of the droplets [1]; this is shown schematically in figure 3 (a). In the unstretched film, the droplet directors, $\hat{N}$, which coincide with the line connecting the boojums and characterize the preferential molecular orientation in the droplet, had a

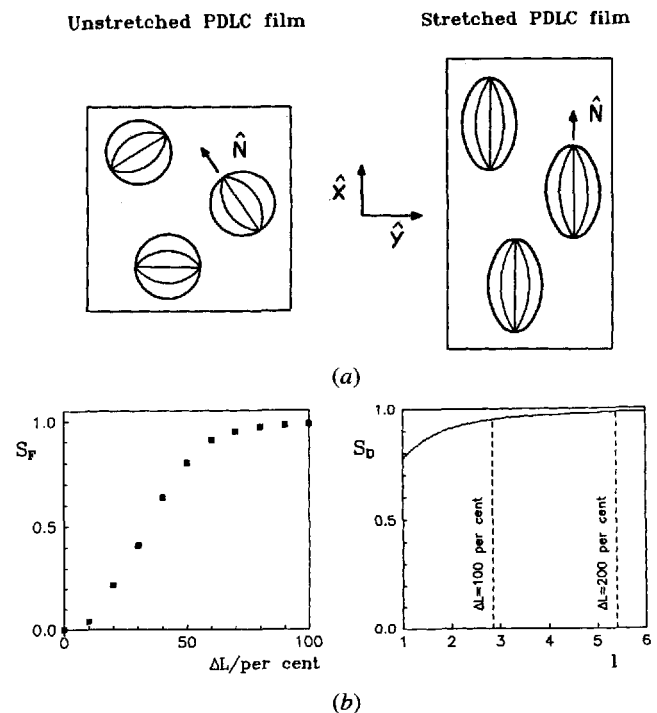Figure 3. (a) Schematic representation of the orientation of bipolar nematic droplets in the unstretched and highly stretched PDLC films. (b) The experimental dependence of the PDLC film order parameter, S_F, on the relative film elongation, ΔL, and the dependence of the droplet order parameter, S_D, calculated for the case of ellipsoidal droplet shape, on the droplet aspect ratio, l.
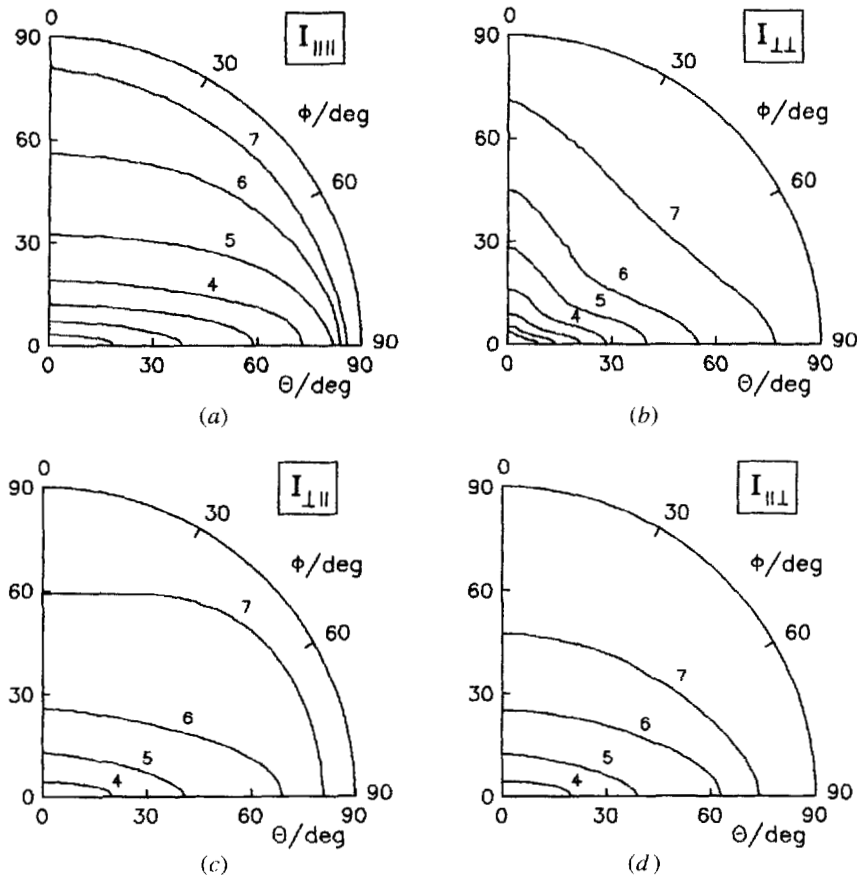
Figure 4.   Scattering diagrams of principal intensities, (a) $I_{||}$, (b) $I_{\perp\perp}$, (c) $I_{\perp||}$ and (d) $I_{||\perp}$ for scattering by the stretched PDLC film into the forward hemisphere. The relative elongation of the sample is 200 per cent with respect to the initial film length. The data are represented in polar coordinates by lines of constant intensity (isophotes). The intensities of the isophotes, normalized to the intensity of the incident beam, are 3×10^{-4}, 10^{-4}, 3×10^{-5}, 10^{-5}, 3×10^{-6}, 10^{-6}, and 3×10^{-7}, 10^{-7} for lines 1 through 7, respectively. One quadrant is shown; the others are symmetric.

random azimuthal orientation and were confined to the film plane due to the oblate shape of droplet cavities [11].

Upon stretching, the droplet cavities were elongated to form prolate ellipsoids with major, a, and minor, b, semi-axes and altered such that $a = a_0 p$ and $b = a_0 p^{-0.5}$, where a_0 is the initial radius of a droplet and p is the extension ratio defined as the ratio of the local film length in the stretched and unstretched states. The droplet directors then preferred to orient along the major axes of the ellipsoids because the elastic energy of the bipolar nematic structure is a minimum in this position. The detailed treatment of the droplet ordering process is beyond the scope of this paper and will be published separately. Here we only give information on the film order parameter, S_F, which is introduced as

$$S_F = \langle 2(\hat{\mathbf{N}}\hat{\mathbf{x}})^2 - 1 \rangle, \qquad (3)$$

where $\hat{\mathbf{x}}$ is the unit vector along the X coordinate axis and the brackets indicate the average over all droplet orientations that occur. (Such a definition of S_F is conditioned by the fact that the droplet directors $\hat{\mathbf{N}}$ are confined to two dimensions and, therefore, for random orientation $\langle (\hat{\mathbf{N}}\hat{\mathbf{x}})^2 \rangle = \frac{1}{2}$ and $S_F = 0$, and for perfect orientation $\langle (\hat{\mathbf{N}}\hat{\mathbf{x}})^2 \rangle = 1$ and $S_F = 1$.) Experimentally, the average $\langle (\hat{\mathbf{N}}\hat{\mathbf{x}})^2 \rangle$ was determined as

$$\langle (\hat{\mathbf{N}}\hat{\mathbf{x}})^2 \rangle = \sum_i f_i (\hat{\mathbf{N}}\hat{\mathbf{x}})^2, \qquad (4)$$

where f_i is the measured orientational distribution function for the droplet directors, represented in a discrete histogram format, and the summation is over all the histogram bins [17]. The dependence of S_F on the relative elongation, ΔL, is shown in figure 3 (b). As is clearly seen, the axes $\hat{\mathbf{N}}$ of the droplet structures were nearly perfectly
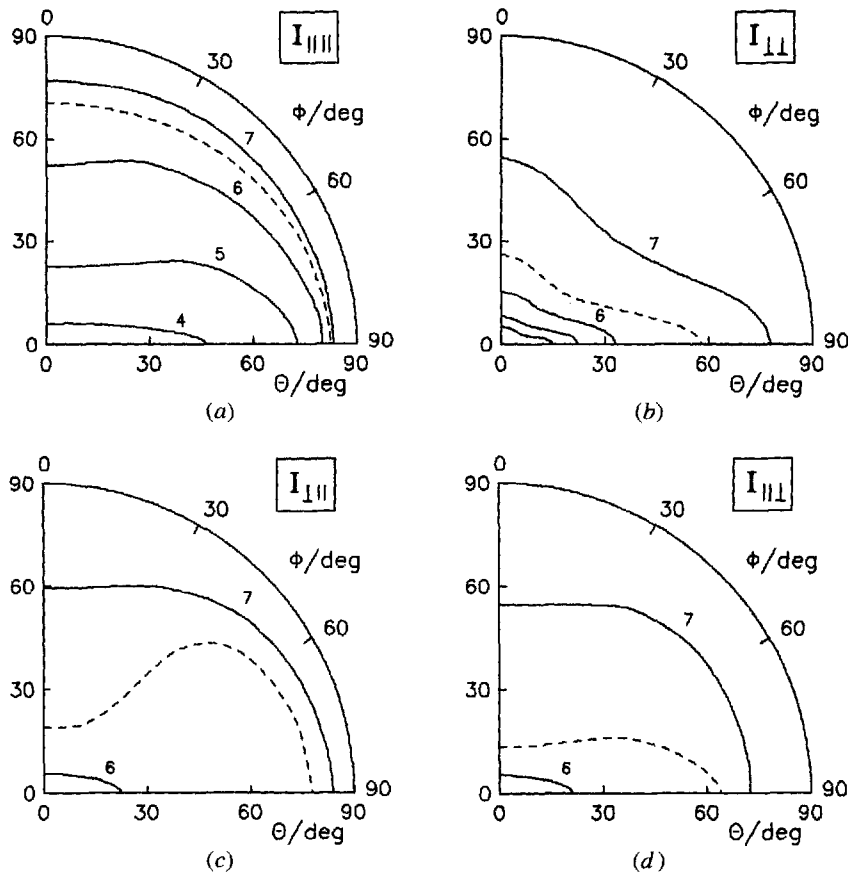
Figure 5. Scattering diagrams of principal intensities, (a) $I_{\|\|}$, (b) $I_{\perp\perp}$, (c) $I_{\perp\|}$ and (d) $I_{\|\perp}$ for scattering into the backward hemisphere. The relative elongation of the PDLC film is 200 per cent. The labelling of intensity lines is the same as in figure 3, but the scattering angle, θ, is reckoned from the backward direction. The dashed curves for $I_{\perp\|}$ and $I_{\|\perp}$ correspond to the supplementary intensity level of 5×10^{-7}.

ordered along the common direction $\hat{x}$ at $\Delta L = 100$ per cent.

The resulting morphological changes were primarily concerned with the modifications in the bipolar director field structure inside the ellipsoidal droplets. To characterize this process quantitatively, using the numerical minimization of droplet free energy in one constant approximation and for strong tangential surface anchoring, we have calculated the dependence of the droplet order parameter, S_D, on the aspect ratio of ellipsoid, $l = a/b$. S_D was defined as

$$S_D = \langle (3(\hat{N}\hat{n})^2 - 1)/2 \rangle,$$ (5)

where $\langle ... \rangle$ stands for the average over a droplet volume and $\hat{n}$ is the local nematic director; the droplet cavity is assumed, for simplicity, to be an ellipsoid of revolution. The relevant data are presented in figure 3 (b). The growth of non-sphericity does not change the general features of the structure, and only the degree of director orientation in the droplet: the LC molecules tend to align along the

droplet major axis so that the distribution of $\hat{n}$ becomes more uniform. At the same time, the dependence $S_D(l)$ suggests that, even at high elongations, the director field remains somewhat distorted, especially at regions near boojums.

4.2. Consideration of light scattering mechanisms

As is obvious from figures 4–9, the stretching of a PDLC film induces drastic changes in light scattering. The scattering patterns are modified from the axially symmetric to patterns which are extended perpendicular to the stretch direction, and, simultaneously, a dramatic redistribution of energy of the scattered light between the principal scattered components is observed (see figures 8 and 9 for a vivid illustration). One half of unpolarized incident light is nearly completely scattered in the form of the $I_{\|\|}$ intensity, whereas approximately 70 per cent of the $\perp$-polarized incident component passes through the sample without scattering. At the same time, only a few per cent of the incident light energy is scattered in the form
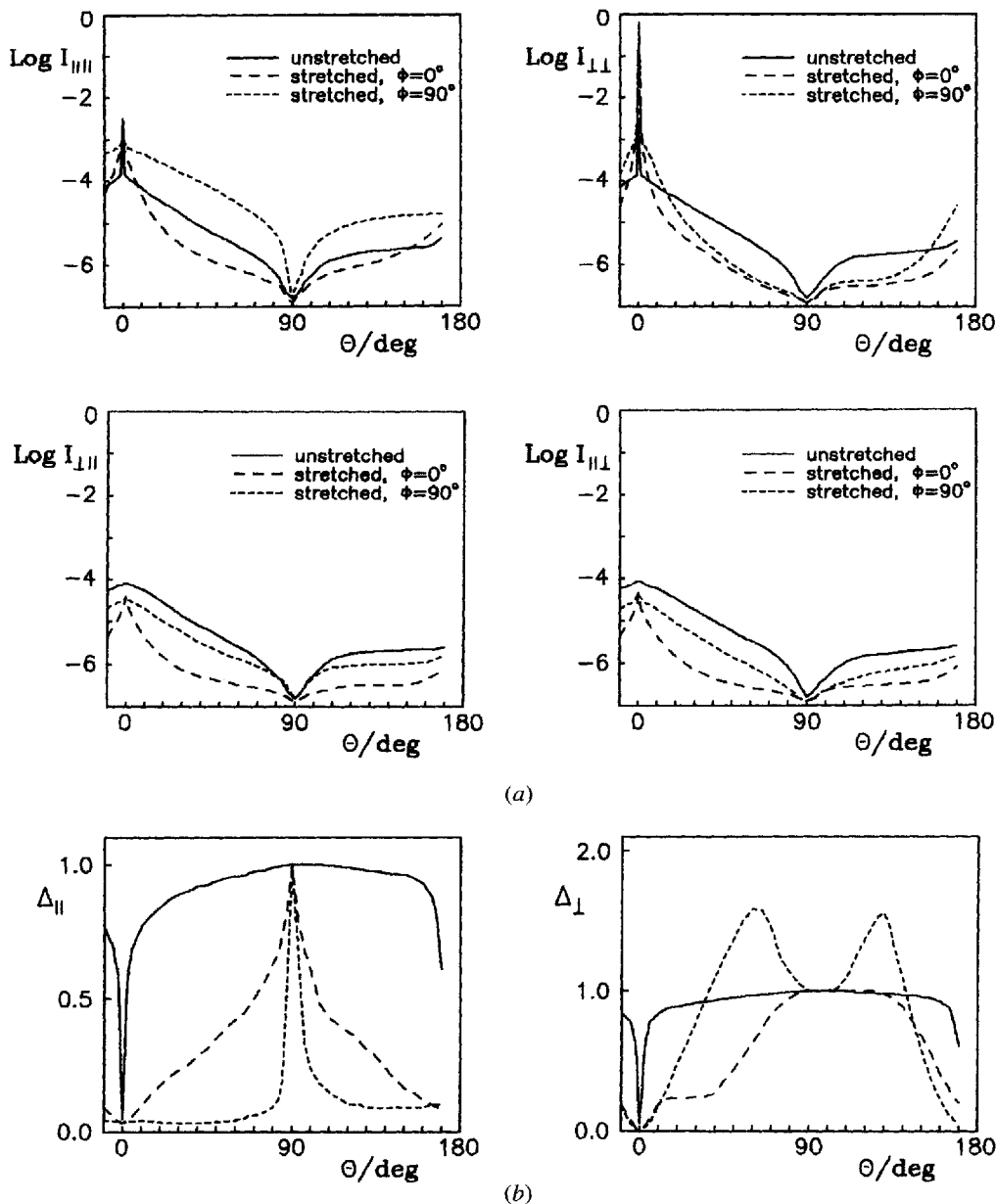
Figure 6.   (a) Principal scattered intensities, $I_{\|\|}$, $I_{\perp\perp}$, $I_{\perp\|}$, $I_{\|\perp}$, and (b) corresponding coefficients, $\Delta_\|$ and $\Delta_\perp$, as functions of scattering angle, θ, for the meridional ($\phi = 0°$) and equatorial ($\phi = 90°$) scattering planes. The solid curves are for the unstretched PDLC sample, and the dashed curves are for the stretched PDLC film with 200 per cent relative elongation. Halves of the angular spectra are shown; the other halves (in the range $-170° \leqslant \theta \leqslant 0°$) are symmetric. All data are normalized with respect to the corresponding incident laser intensity at $\theta = 0°$.

of cross-polarized components, $I_{\perp\|}$ and $I_{\|\perp}$, which are similar to each other in magnitude, but are substantially suppressed compared to the respective intensities for the unstretched PDLC sample. On the whole, the highly stretched PDLC film transmits about 35 per cent of the unpolarized incident radiation, while the other fraction is scattered.

The observed growth of macroscopic optical anisotropy of the system can be reasonably interpreted on the basis

of the morphological modifications discussed in § 4.1. For the case of the random azimuthal alignment of droplet directors in the unstretched sample, the scattering efficiency of the film for an arbitrary component of the incident light can be reduced, as a first approximation, to that of a collection of isotropic spherical droplets with refractive indices n_{rand} lying in the range from n_o to n_e:

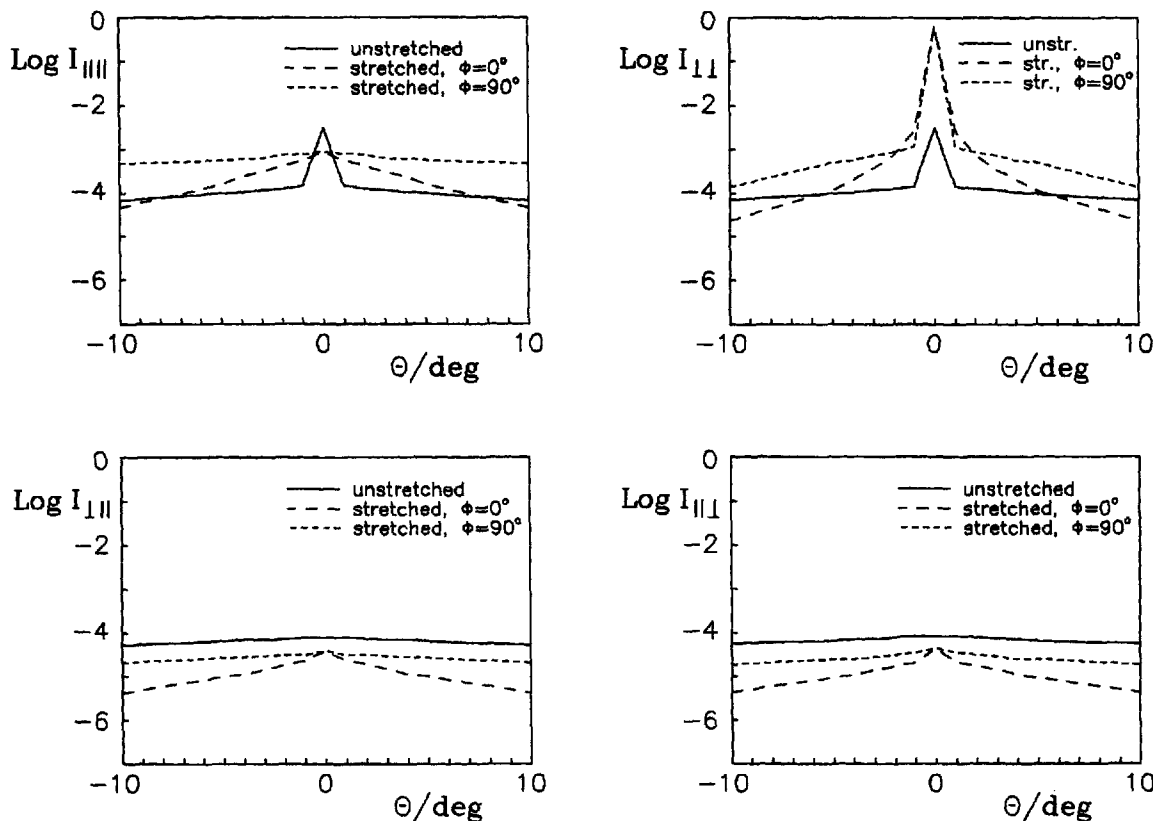$$n_e > n_{rand} > n_o \approx n_m. \tag{6}$$

Figure 7. Expanded view of figure 6(a) at small scattering angles.

Because of this, the scattering is insensitive to the polarization of incident radiation (see [14,18] for a detailed discussion). When the film becomes ordered upon stretching, the liquid crystal molecules in the elongated scattering domains are preferentially aligned along the

Figure 8. Principal intensities for the light transmitted through the sample ($\theta = 0°$) as functions of relative film elongation, ΔL.

common direction so that the effective refractive index for the $\|$-polarized incident light, $n_\|^{\text{eff}}(p)$, approaches n_e, the value most different from n_m:

$$n_e > n_\|^{\text{eff}}(p) > n_{\text{rand}}, \qquad (7)$$

while the average refractive index for the $\perp$-polarized component, $n_\perp^{\text{eff}}(p)$, becomes similar to n_o:

$$n_{\text{rand}} > n_\perp^{\text{eff}}(p) \geqslant n_o \approx n_m. \qquad (8)$$

These changes result in a difference in scattering for $\|$- and $\perp$-polarized incident light. The process of index matching/ mismatching with stretching can be divided into the two principal stages. The main contribution arises from the orientational ordering of the droplet directors $\hat{N}$, which is completed at $\Delta L = 100$ per cent ($S_F \to 1$; see figure 3 (b)). This stage readily correlates with the dependencies of the principal film transmittances of the ΔL shown in figure 8. Later in the process, the alteration of the effective refractive indices is completely determined by increasing the order of the LC molecules inside the droplet: ($\hat{N}\hat{n}$) → 1 in most parts of the droplet with increase of its non-sphericity (see the dependence $S_D(l)$ in figure 3 (b)). Note that for the droplets under consideration ($2a \gg \lambda$), the non-spherical shape of a droplet is not relevant in determining the droplet optical anisotropy (the so-called form anisotropy [12]), this being entirely determined by the
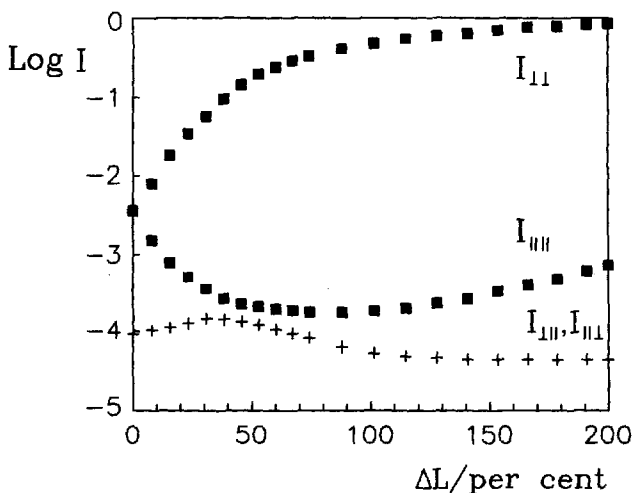
O. A. Aphonin

$\phi=0°$

$I_{||||}$

40

Relative elongation,
per cent
——— 0
— — — 100
········ 200

20

$\phi=90°$

0

0   20   40   60   80

Θ/deg

(a)

$\phi=0°$

$I_{\perp\perp}$

40

Relative elongation,
per cent
——— 0
— — — 100
········ 200

20

$\phi=90°$

0

0   20   40   60   80

Θ/deg

(b)

$\phi=0°$

$I_{\perp||}$

40

Relative elongation,
per cent
——— 0
— — — 100
········ 200

20

$\phi=90°$

0

0   20   40   60   80

Θ/deg

(c)

$\phi=0°$

$I_{||\perp}$

40

Relative elongation,
per cent
——— 0
— — — 100
········ 200

20

$\phi=90°$

0

0   20   40   60   80

Θ/deg

(d)
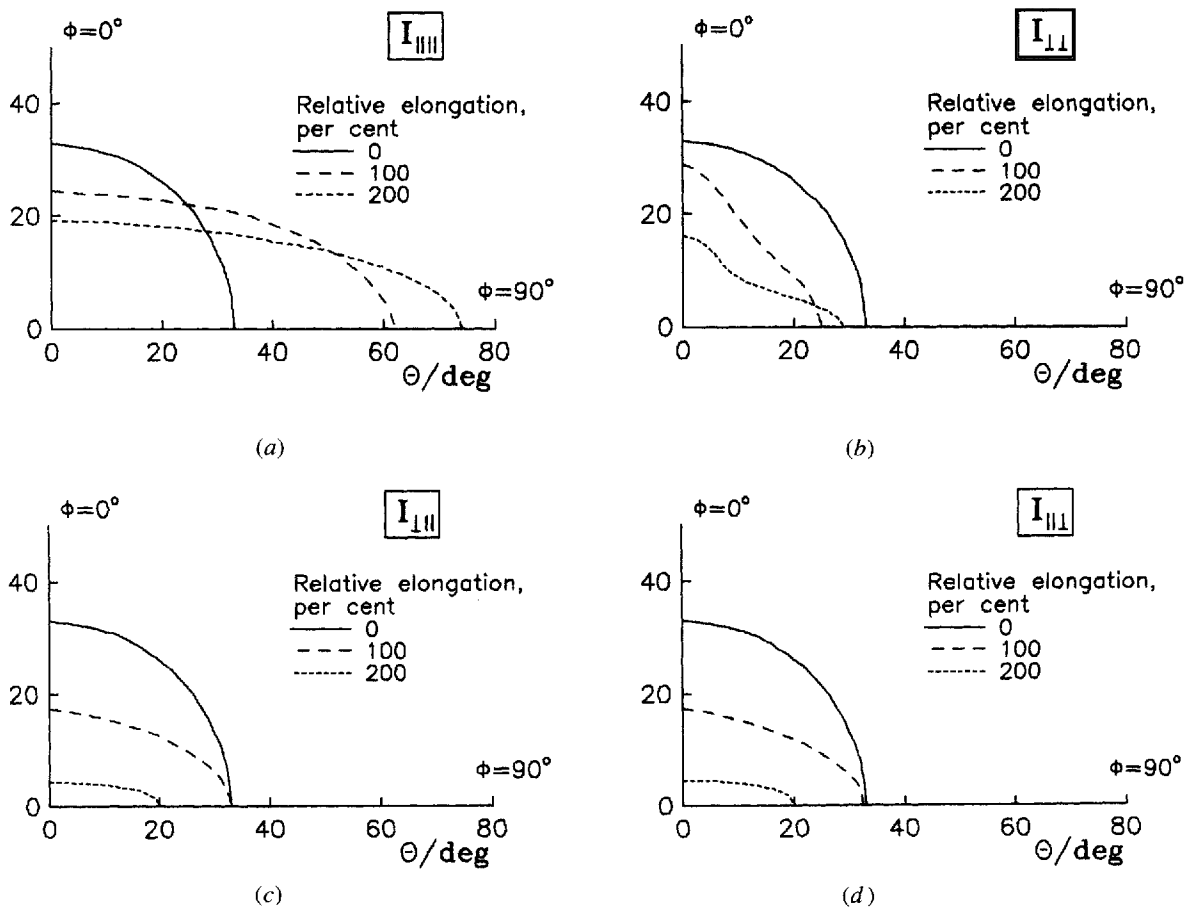
Figure 9. Effect of stretching on the energy redistribution between the principal scattered intensities, (a) $I_{||||}$, (b) $I_{\perp\perp}$, (c) $I_{\perp||}$ and (d) $I_{||\perp}$ represented by corresponding isophotes with intensity 10^{-5} for scattering into the forward hemisphere. The solid curves are for the unstretched PDLC film; the dashed curves are for the stretched film.

intrinsic optical anisotropy of the LC director configuration inside the droplet. As a result, the average optical anisotropy of the system, $\Delta n^{\mathrm{eff}}(p) = n_{||}^{\mathrm{eff}}(p) - n_{\perp}^{\mathrm{eff}}(p)$, grows steadily with film elongation up to the limiting value $\Delta n = n_{\mathrm{e}} - n_{\mathrm{o}} \approx 0{\cdot}2$.

Let us now consider more comprehensively the individual scattered components for a perfectly ordered PDLC film ($\Delta L = 200$ per cent). As was mentioned above, the strongest scattering is observed for the $I_{||||}$ component, when the greatest refractive index mismatch occurs ($n_{||}^{\mathrm{eff}} \gg n_{\mathrm{m}}$). The transmitted beam is therefore substantially attenuated compared to that for the unstretched sample: the $I_{||||}$ ($\theta = 0°$) falls from $\approx 2{\cdot}5 \times 10^{-3}$ to $\approx 7 \times 10^{-4}$. The large angle scattering patterns become narrower and elongated along the equatorial plane ($\phi = 90°$) where the $I_{||||}$ angular spectrum is, on average, of a 10 times greater intensity than that for an unstretched film. In contrast, $I_{||||}$ ($\phi = 0°$) is appreciably reduced. The reason for the prevailing equatorial scattering is directly related to the aspect ratio (axes ratio) of the droplets, in compliance with predictions of diffraction theory [15, 19]: if a scattering

object, at normal incidence of the probing light, is symmetrically extended (compressed) along a particular direction by a factor μ, the relevant scattering pattern is compressed (extended) μ times along the same direction, whereas the intensity at a given point of the new pattern becomes μ^2 times greater (smaller) than the intensity at the corresponding point of the original pattern. This is principally obeyed for the samples examined at small scattering angles, where the isophotes have a perfect ellipsoidal shape with the aspect ratio very similar to that of the droplets ($l \approx 5{\cdot}4$).

As to the rate of decrease of the scattered intensity with scattering angle (i.e. $\partial I/\partial\theta$), theory predicts [12, 19, 20] that, for the relatively large scattering objects under consideration and for a single scattering regime, at least 95 per cent of the scattered radiation should be confined to a narrow cone around the forward direction with half-angle $\delta(\phi) \approx 2\arcsin[2{\cdot}5/k\bar{a}\,(\phi)]$, where $k\bar{a}\,(\phi)$ stands for the conventional, azimuthally dependent, diffraction size parameter averaged over a droplet size distribution ($k = 2\pi n_{\mathrm{m}}/\lambda$). For the samples studied with $k\bar{a}\,(\phi)$ varying

between the limiting values $k\bar{a} \approx 65$ at $\phi = 0°$ and $k\bar{a} \approx 12$ at $\phi = 90°$, the corresponding estimate gives δ $(\phi = 0°) \approx 6°$ and $\delta(\phi = 90°) \approx 30°$. However, as seen from figure 6, the measured intensities fall off much more weakly with increasing scattering angle. Furthermore, for $k\bar{a}$ $(\phi) \gg 1$, the back scattering should be negligible, because $I(\theta \rightarrow 180°)/I(\theta \rightarrow 0°) \propto [k\bar{a}\,(\phi)]^{-4}$ according to theory. The expected ratio of back to forward scattering should be no more than 10^{-4}, while the experimental value is no less than 10^{-1}. The primary reason for these discrepancies is apparently concerned with the multiple scattering of light by closely packed droplets, which, as in the case of common unstretched PDLC films [14,21], significantly contributes to the overall scattering process in the stretched PDLC samples. Succeeding scattering events of higher orders redirect more and more of the primary scattered light to large angle up to the backward direction, thus leading to the substantial enhancement of the wide angle and back scattering observed experimentally. An additional contribution to this process arises from the scattered light totally internally reflected at the planar sample–air interfaces at angles $41° \leqslant |\theta_i| \leqslant 139°$ (where θ_i is the scattering angle inside the sample) and therefore scattered again [14].

As a consequence of the best index match ($n_{\perp}^{\text{eff}} \approx n_{\text{m}}$), the transmittance for the $I_{\perp\perp}$ component is extremely high, reaching the value of 0·7, whereas the forward off-scattering is substantially reduced. It is remarkable that the corresponding $I_{\perp\perp}$ diagrams exhibit two clearly defined reflexes in the equatorial and meridional scattering planes. A reasonable explanation of such a behaviour can be obtained from conventional SALS theory [22]. In the context of this theory the effective refractive index of a scatterer, n^{eff}, used previously in the discussion, is broken into the isotropic and anisotropic parts. As a result, the $I_{\perp\perp}$ intensity (which, in essence, is the V_v pattern obtained in the SALS experiment) can be represented as a sum of two contributions

$$I_{\perp\perp} \approx A(\theta, k\bar{a}\,(\phi), l, n_o - n_m) + B(\theta, \phi, S_D, n_e - n_o). \quad (9)$$

The first, 'isotropic' term arises from the difference between the smallest refractive index of the material comprising the droplet, n_o, and that of the surroundings, n_m, and describes the scattering from a droplet as if it was an isotropic object with index n_o and of identical size and shape ($k\bar{a} \approx 65$, $k\bar{b} \approx 12$, $l \approx 5·5$). Experimentally, this is responsible for the *equatorial* component in $I_{\perp\perp}$ diagrams. The second term in equation (9) arises entirely from the optical anisotropy of the liquid crystal $\Delta n = n_e - n_o$ and represents the scattering from intra-droplet domains involving dipoles induced by linearly polarized incident light along the long axis of LC molecules. Since the induced dipole moment is proportional to $\hat{n} \cdot \hat{e}_{\perp i}$, where $\hat{n}$ is the local nematic director and $\hat{e}_{\perp i}$ is the electric vector

of the $\perp$-polarized incident light (see figure 1), it is apparent that the dipoles are induced only in polar regions of the bipolar nematic droplet where the director field lines radiate outward from boojums, and, $\hat{n} \cdot \hat{e}_{\perp i}$ substantially differs from zero. A non-uniform director distribution in the regions near boojums is illustrated quantitatively in figure 10 (a). As shown schematically in figure 10 (b), the resulting scattering domains are extended predominantly in the direction perpendicular to the long droplet axis, having a size comparable to the light wavelength ($\approx 0·5\,\mu m$). (An 'effective' extension of the domain along the equatorial plane is further increased after the scattered light passes through the analyser since in this case the power received by the detector is proportional to $(\hat{n} \cdot \hat{e}_{\perp i})^4$ [22].) Because, according to SALS theory, the strongest scattering should be in the plane perpendicular to the direction of the greatest dimension of the domain [22], the corresponding scattering pattern, averaged over all the droplets in the incident beam, is extended vertically in the *meridional* plane. It should be noted that in the case of $I_{\parallel\parallel}$ component, the anisotropic term in scattering dominates, since the vectors $\hat{n}$ and $\hat{e}_{\perp i}$ are nearly parallel in the greater part of the droplet. As a result, the induced highly scattering dipoles form a domain occupying the whole droplet volume; this enables the $I_{\parallel\parallel}$ scattering to be treated in terms of diffraction theory as was done above. An alternative view on the origin of the meridional scattering is that it can arise from fluctuations in density, average refractive index, and/or degree of crystallinity along the draw axis of the polycrystalline PVA matrix. Although we do not rule out these mechanisms, they seem to play only a negligible role in the samples examined. This statement is supported by experiments on pure, LC-free, stretched PVA/glycerol films which have revealed practically no
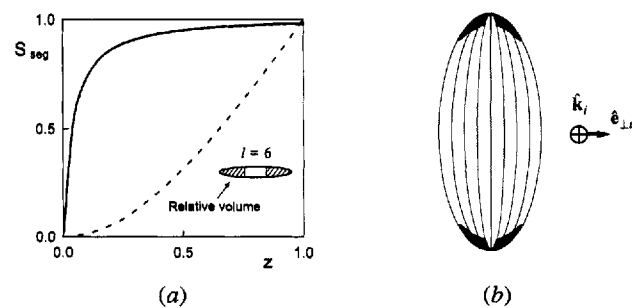

Figure 10. (a) Calculated order parameter of a droplet segment (shown in inset), S_{seg}, as a function of the relative segment size, z, defined as the ratio of the segment height to the major semi-axis of the droplet. The droplet aspect ratio is $l = 6$. Also shown is the corresponding alteration of the segment relative volume (dashed curve). (b) Schematic representation of polar droplet regions where the scattering dipoles associated with the LC birefringence anisotropy are induced. Axial cross-section is shown.

scattering in comparison with the stretched PDLC samples.

The observed reduction in the amount of $I_{\perp\parallel}$ and $I_{\parallel\perp}$ scattering is obviously related to the fact that the LC molecules in the droplets become more aligned in the stretch direction with increase in S_F and S_D and, therefore, the intra-droplet phase shifts and polarization rotations of the linearly polarized incident light are substantially reduced. As a consequence, the scattered light has a considerable degree of linear polarization and is effectively quenched by a crossed analyser. Nevertheless, the depolarization is still significant due to (1) remaining distortions of the bipolar nematic structure inside the droplets and (2) a multiple scattering contribution. As for the first of these two effects, the supplementary SALS experiments [23], performed on very thin PDLC films with a very low droplet concentration to minimize the multiple scattering, have shown that the scattering lobes of the four-leaf H_V patterns, occurring for unstretched samples in the 90° interval from $\phi = 45°$, are shifted towards the

equatorial scattering plane, but do not completely disappear, making an angle of about 10° with respect to the equator. Based on the conventional SALS interpretation [22], this gives additional evidence that the director field remains distorted in polar regions of highly elongated bipolar nematic droplets. However, in the samples under consideration this 'fine' structure of the isophotes is masked by multiple scattering; it blurs the SALS patterns and is responsible for the observed isophotes having an ellipsoidal shape at small scattering angles (see figures 4, 5 and 9). The distortion of the isophotes at large scattering angles is probably due to the effect of the birefringence of the stretched PVA/glycerol matrix ($\Delta n_m = n_{\parallel m} - n_{\perp m} \approx 0.03$; see figure 3 from reference [7]), which causes the multiply scattered light propagating within the medium to accumulate phase change; this in its turn produces some ellipticity detected by an analyser. The effect is more pronounced for back scattering, when at least a double passage of the back scattered beam through the sample takes place (compare figures 4 and 5).
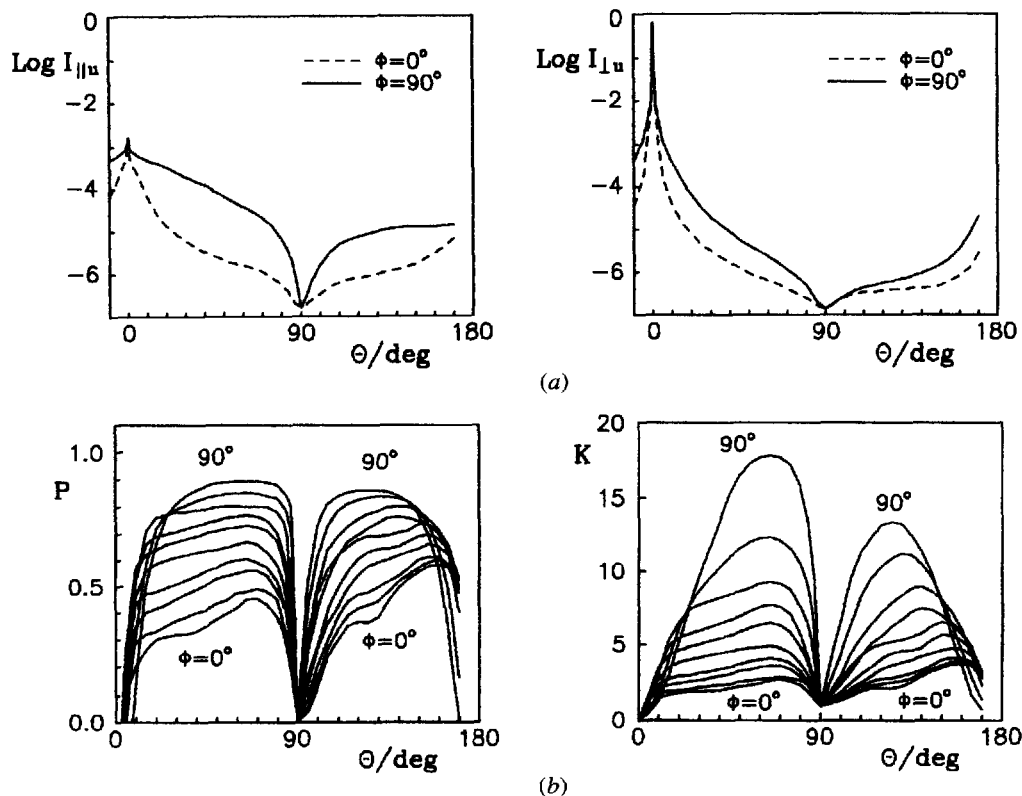

Figure 11.   (a) The scattered intensities, $I_{\parallel u}$, $I_{\perp u}$ and (b) the relevant degree of polarization, P, and intensity ratio, $K = I_{\parallel u}/I_{\perp u}$, as functions of scattering and azimuthal angles for the case of unpolarized incident light. The data for $I_{\parallel u}$, $I_{\perp u}$ are presented only for the principal scattering planes ($\phi = 0°$, 90°), while the data for P and K are presented for 10 degree intervals of azimuthal angle from $\phi = 0°$ to $\phi = 90°$. The region of negative values of P in the neighbourhood of $\theta = 0°$, where $P \to -1$ with decreasing θ, is not shown.

(a)

(b)

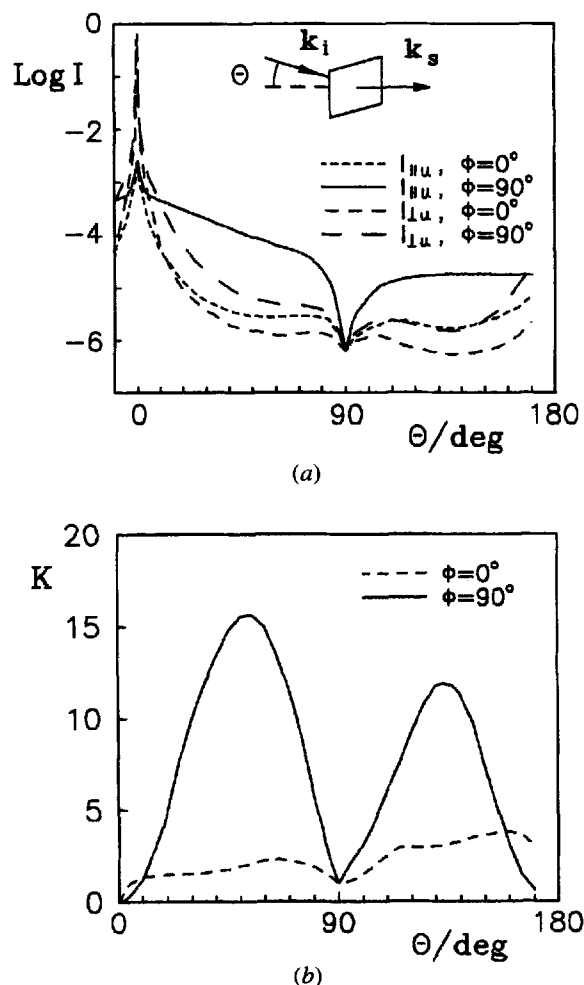Figure 12. (a) The scattered intensities, $I_{\|u}$, $I_{\perp u}$ and (b) the intensity ratio, $K = I_{\|u}/I_{\perp u}$, measured in the direction along the PDLC film normal ($\phi = 0°$), as functions of the incident angle θ_i. The scattering geometry is shown in the inset. All curves are for the principal incidence planes ($\phi = 0°$, $90°$). The relative elongation of the PDLC film sample is 200 per cent.

A more detailed discussion of a similar mechanism may be found in [24]. The values of $\Delta_\perp$ ($\phi = 90°$) greater than unity may be explained in the following way. While the $\perp$-polarized incident light is only weakly scattered after the primary scattering event, the primary $I_{\|\perp}$ component which arises simultaneously (due to depolarization) is scattered more strongly within the equatorial plane. The multiple scattering process rapidly accumulates these differences, causing the resulting $I_{\|\perp}$ intensity to be partially polarized in the $\phi = 90°$ plane.

4.3. Light polarizing properties

The scattering processes discussed above are responsible for the principal polarization components of the incident beam being spatially distributed among

the transmitted and scattered light (see figures 11). The transmitted beam ($\theta = 0°$) becomes partially linearly polarized in the plane perpendicular to the stretch direction. The absolute values of $P(\theta = 0°)$ are therefore very high, attaining ≈ 0.997 for our samples. The same kind of polarization is also observed for the light scattered within a small cone ($|\theta| < 3°-5°$) around the forward direction.

On the contrary, the light scattered out of the direction of the incident beam ($|\theta| > 5°$) is partially polarized in the plane defined by the stretch direction and a given direction of the scattered beam (i.e. the output reference plane). The degree of polarization reaches the maximum values of about 0.9 in the equatorial scattering plane. This correlates with the space distribution of the $I_{\|\|}$ component. For all the azimuthal angles, $P(\theta)$ increases rapidly when θ changes from $\theta = 0°$ or $180°$, but the sharp minima associated with the boundary refraction/reflection are observed at $|\theta| \to 90°$. A good illustrative example is light scattering by a dipole [19], the radiation from which is concentrated in the plane perpendicular to the dipole axis (direction of stretching) and polarized in the meridional planes. Unlike the P ($\theta = 0°$), which may have an optimum at intermediate values of ΔL [7], the P ($\theta > 0°$) were found to increase monotonically with stretching.

5. Potential display applications

One possibility, which was discussed partly in [2, 7], consists in using a PDLC scattering sheet polarizer with high light power densities in the transmission mode (powerful lasers, LC projection systems, etc.). Because the unwanted polarization component is scattered rather than absorbed, the heat generation in a PDLC polarizer is greatly minimized, allowing it to withstand light power densities of the order of kilowatts per cm^2. The principal transmittances for $\perp$- and $\|$-polarized components of collimated incident light, attained in our laboratory ($T_\perp \geqslant 0.7$ and $T_\| \leqslant 7 \times 10^{-4}$; see figure 8) are comparable to the values for conventional dichroic sheet polarizers. Besides this, PDLC polarizers exhibit fairly good spectral characteristics: $T_\perp$ and $T_\|$ are nearly independent of light wavelength in the visible region, and the polarizers maintain a substantial polarizing ability at wavelengths up to 2 μm and over [23]. The regular principal transmittance ratio, $T_\perp/T_\| \approx 10^3$, can be further increased up to 10^4 or even more by employing the spatial filtering technique [25], which enables minimization of $T_\|$ without noticeable reduction in $T_\perp$.

Another possibility based on the polarization properties of the scattered light is to utilize a stretched PDLC film as a polarizing diffuser for back-lit direct view twisted nematic LC displays (LCDs). In such a construction, the PDLC film, placed on the rear surface of the twisted nematic LC-cell and oriented along one of the two

principal cell directions, can combine the functions of both the isotropic diffuser and back polarizer in a conventional LCD. The display can be switched from the scattering state, when it appears white due to transmission of the polarized scattered light through the front polarizer, to a nearly non-scattering state, when the display appears transparent and the viewer sees the scene behind the LCD. The back scene may be black or coloured to produce a black and white or a coloured display. Additionally, dichroic or fluorescent dyes may be incorporated into the PDLC film to realize a two-colour LCD. The application discussed is illustrated by figure 12, which shows the scattered intensities $I_{\|u}$ and $I_{\perp u}$ (unpolarized incident light) and the intensity ratio, $K = I_{\|u}/I_{\perp u}$ (that may be treated as a contrast ratio), measured in the direction along the film normal, as functions of the incident angle θ_i, varied in the range from perpendicular to nearly grazing incidence. As is clearly seen, the illumination source should be place in the plane of incidence with $\phi = 90°$ (perpendicular to the stretch direction). Reasonable values of K ($\geqslant 10$) are achieved at $30° \leqslant \theta_i \leqslant 70°$ for the back-lit mode, and at $120° \leqslant \theta_i \leqslant 145°$ for the front-lit mode with optima at $\theta_i \approx 55°$ and $135°$, respectively. An estimation of the ranges of viewing angle about the film normal in the back-lit mode gives (for the criterion $K \geqslant 5$) $\pm 25°$ and $\pm 30°$ for viewing planes with $\phi = 0°$ and $90°$, respectively. These values are comparable to the viewing angles of conventional twisted nematic LCDs.

In closing, it should be noted that many results presented in this paper are quite general and applicable to any anisotropic light scattering PDLC system having the symmetry D_{2h}.

The author is indebted to D. A. Yakovlev for helpful discussions and to Yu. V. Panina for preparing the PDLC film samples.

References

[1] DOANE, J. W., 1990, *Liquid Crystals: Applications and Uses*, edited by B. Bahadur (World Scientific), Chap. 14, and references therein.

[2] DOANE, J. W., CHIDICHIMO, G., and VAZ, N. A., 1987, U.S.A. Patent No. 4688900.

[3] MARGERUM, J. D., LACKNER, A. M., RAMOS, E., LIM, K.-C., and SMITH, W. H., 1989, *Liq. Crystals*, **5,** 1477.

[4] HIKMET, R. A. M., 1990, *J. appl. Phys.*, **68,** 4406; 1991, *Liq. Crystals*, **9,** 405.

[5] KITZEROW, H.-S., MOLSEN, H., and HEPPKE, G., 1992, *Appl. Phys. Lett.*, **60,** 3093.

[6] SHIMADA, E., and UCHIDA, T., 1992, *Jap. J. appl. Phys. Pt. 2B*, **31,** 352.

[7] APHONIN, O. A., PANINA, YU. V., PRAVDIN, A. B., and YAKOVLEV, D. A., 1993, *Liq. Crystals*, **15,** 395.

[8] ZYRYANOV, V. YA., SMORGON, S. L., and SHABANOV, V. F., 1993, *Pis'ma Zh. eksp. teor. Fiz.*, **57,** 17.

[9] LEE, K., SUH, S.-W., and LEE, S.-D., 1994, *Appl. Phys. Lett.*, **64,** 718.

[10] DRZAIC, P. S., 1986, *J. appl. Phys.*, **60,** 2142.

[11] DRZAIC, P. S., 1988, *Liq. Crystals*, **3,** 1543.

[12] BOHREN, C. F., and HUFFMAN, D. R., 1983, *Absorption and Scattering of Light by Small Particles* (Wiley), Chap. 13.

[13] NEWTON, R., 1966, *Scattering Theory of Waves and Particles* (McGraw Hill), Chap. 1.

[14] MONTGOMERY, G. P., 1988, *J. opt. Soc. Am. B*, **5,** 774.

[15] BORN, M., and WOLF, E., 1964, *Principles of Optics* (Pergamon Press).

[16] CHEN, G.-P., TAKEZOE, H., and FUKUDA, A., 1989, *Jap. J. appl. Phys.*, **28,** 56.

[17] APHONIN, O. A., *Molec. Crystals liq. Crystals* (submitted).

[18] ZUMER, S., GOLEMME, A., and DOANE, J. W., 1989, *J. opt. Soc. Am. A*, **6,** 403.

[19] VAN DE HULST, H. C., 1957, *Light Scattering by Small Particles* (Wiley).

[20] ZUMER, S., 1988, *Phys. Rev. A*, **37,** 4006.

[21] WEI WU, KELLY, J. R., 1992, *14th International Liquid Crystal Conference*, Pisa, Abstracts, p. 774.

[22] STEIN, R. S., and RHODES, M. B., 1960, *J. appl. Phys.*, **31,** 1873; CLOUGH, S., VAN AARSTEN, J. J., and STEIN, R. S., 1965, *J. appl. Phys.*, **36,** 3072; RHODES, M. B., and STEIN, R. S., 1969, *J. polym. Sci.*, Part A-2, **7,** 1539.

[23] APHONIN, O. A., unpublished results.

[24] STIDHAM, S. N., and STEIN, R. S., 1966, *J. polym. Sci.*, Part A-2, **4,** 89; BOOTS, H. M., 1994, *J. opt. Soc. Am. A*, **11,** 2539.

[25] CAULFIELD, H. J., and SOREF, R. A., 1971, *Appl. Phys. Lett.*, **18,** 5.